Heliyon 5 (2019) e02420

Contents lists available at ScienceDirect

Heliyon

journal homepage: www.heliyon.com

Computational and spectral studies of 3,3'-(propane-1,3-diyl) bis(7,8-dimethoxy-1,3,4,5-tetrahydro-2H-benzo[d]azepin-2-one)

S. Anil Kumar, B.L. Bhaskar *

Department of Chemistry, Amrita School of Engineering, Bengaluru, Amrita Vishwa Vidyapeetham, India

ARTICLE INFO

Keywords:
Analytical chemistry
Pharmaceutical chemistry
Ivabradine impurity
Computational
DFT
FTIR
ADME studies

ABSTRACT

Detection and qualification of unknown impurities during commercial drug synthesis have been mandated by the regulatory authorities. 3,3'-(propane-1,3-diyl)bis(7,8-dimethoxy-1,3,4,5-tetrahydro-2H-benzo [d]azepin-2-one) in short IVA-9, is one such process-related impurity formed during the synthesis of cardiotonic drug Ivabradine. The structure and properties of this molecule have not been explored yet. A suggestive reaction route for the chance formation of IVA-9 during the commercial synthesis of parent drug molecule has been reported in this article. Further, the optimized geometry and vibrational studies have been computed using Gaussian 09. Experimental FTIR scan has also been performed and values show satisfactory consilience with the computational data. The frontier orbital energies and energy band gaps of the reaction fragments and products were computed. The evaluation of ADME parameters such as absorption, distribution, metabolism, and excretion are performed using SwissADME tool to assess the drug-likeness and medicinal chemistry friendliness. Six physiochemical parameters namely flexibility, lipophilicity, size, polarity, solubility and saturation and their critical limits are depicted using the bioavailability radar of the programme to provide insights into pharmacokinetic properties such as human gastrointestinal absorption (HIA), blood-brain-barrier (BBB) permeability, total polar surface area (TPSA) and inhibitor action to important cytochromes etc.

1. Introduction

Impurity profiling is an important subset of the pharmacological drug development programme. Presence of impurity molecules in the pharmaceutical formulations might influence the therapeutic compliance and even jeopardize the safety and efficacy of drugs. Historically, impurity is any substance that impacts the percentage purity of the matter of interest like an active ingredient or drug material. However, these impurities do not necessarily affect the quality negatively all the time. Having said that, the purity of the active pharmaceutical ingredient (API) would be compromised, notwithstanding whether the impurity has superior pharmacological or toxicological property. Therefore, any foreign material-whether inert, toxic or pharmaceutically superior-must be thoroughly analyzed and accounted for [1]. 3,3'-(propane-1,3-diyl)bis(7, 8-dimethoxy-1,3,4,5-tetrahydro-2H-benzo [d]azepin-2-one) (IVA-9) is an impurity produced during the commercial synthesis of cardiotonic drug Ivabradine. Ivabradine is a negative chronotropic drug which helps to lower heart rate without many adverse effects [2]. The natural pacemaker of the heart, also known as the sinoatrial node, undergoes spontaneous depolarization due to the recurring changes in its membrane potential [3]. Ivabradine functions by controlling the percolation of sodium-potassium ions through the hyperpolarisation-activated cyclic nucleotide-gated (HCN) channels or the 'f' channels. This sodium-potassium current initiates the diastolic depolarization and hence is responsible for the pacemaker current. Ivabradine selectively blocks the ions flow through the HCN channels by physically binding on to these channels and this result in a reduced pacemaker current. A lowered pacemaker current ensures a reduced heart rate, dependent on the drug dosage [4]. Though sufficient information is available about the structure, properties [5, 6, 7], and estimation techniques [8, 9, 10, 11, 12, 13, 14, 15] of Ivabradine; there is little information available about its impurity molecule IVA-9 (Fig. 1a & 1b). The spectroscopic and volumetric estimation of the title molecule has been studied recently by the same authors [16]. At times, the exploratory studies of such molecules lead to the development of alternate drug molecules with better pharmacodynamics or help us to assess its toxicity impact. This has prompted the authors to undertake the structural and spectral studies of IVA-9 via experimental and computational approaches to assess the structure-property relationship. The primary screening of the physiochemical properties was also performed to assess and compare the

* Corresponding author.
E-mail addresses: bl_bhaskar@blr.amrita.edu, basee77@gmail.com (B.L. Bhaskar).

https://doi.org/10.1016/j.heliyon.2019.e02420
Received 25 June 2019; Received in revised form 19 August 2019; Accepted 2 September 2019

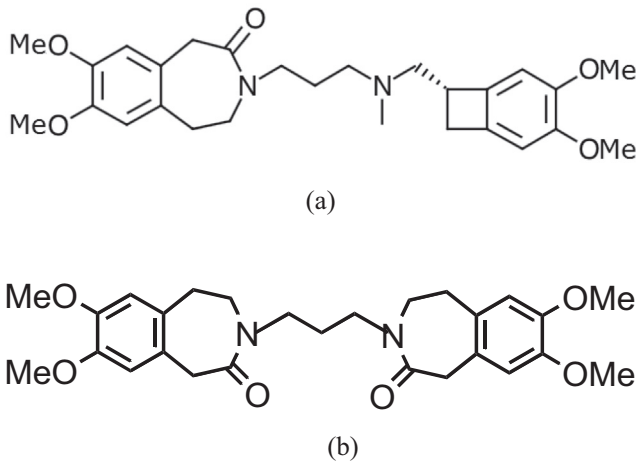

Fig. 1. (a): Ivabradine. (b): IVA-9.

drug-likeness and toxicity effects vis-a-vis the parent drug. The authors are hopeful that these results might help in the future studies wherein IVA-9 could be explored as a potential drug molecule with good pharmacological properties and minimum toxicological impacts.

2. Materials and methods

3,3'-(propane-1,3-diyl)bis(7,8-dimethoxy-1,3,4,5-tetrahydro-2H-benzo [d]azepin-2-one) received as a gift sample was used as received. Shimadzu IRSpirit Fourier Transform Spectrophotometer was used for vibrational analysis of the sample between 4000-400 cm^{-1} with a resolution of 2 cm^{-1}. Computational studies were performed using Gaussian 09 [17] and Gaussview 06 interface on VMware 8 core virtual CPU (Dell Power Edge R740 server). The optimized geometry, the geometrical parameters, and the vibrational spectrum were computed using Density Functional Theory (DFT) at basis set B3LYP/6-311g. SwissADME, a web-based tool is used to study the physiochemical aspects to assess the drug-likeness and pharmacokinetics of IV-9 [18]. The SwissADME web tool can be accessed freely via http://www.swissadme.ch.

3. Results

3.1. Synthetic route for ivabradine and chance formation of IVA-9 as an impurity

The routine synthesis of Ivabradine involves the reaction of 7,8-dimethoxy-1,3-dihydrobenzo(d)azepin-2-one (I) with dimethyl formamide to form 7,8-Dimethoxy-3-(3-chloropropyl)-l, 3-dihydro-2H-3-benzazepin-2-one (II) which is then converted to its iodo-derivative (III). The compound III undergoes coupling with (lS)-4,5-Dimethoxy-l-[(methylamino) methyl]benzocyclobutane hydrochloride followed by selective hydrogenation to yield Ivabradine (Fig. 2) [19].

Though, IVA-9 was not a listed by-product of this reaction, the possibility of its chance formation as an impurity during commercial synthesis has been described by the following reaction route (Fig. 3).

3.2. Structural elucidation

The parent drug Ivabradine is a horse-shoe shaped molecule made up of two unsymmetrical bicyclic moieties (Fig. 4); first part containing a seven-member lactam unit whereas the latter has a cyclobutane part [5].

However, the impurity molecule is expected to be different from the parent molecule as it is formed by the dimerization of two lactam bearing segments connected via an alicyclic linkage. The structure is symmetric between two benzazepine units without the tertiary amino nitrogen. Computational modeling has emerged as a powerful tool to elucidate structural and spectral properties of unexplored molecules. The geometry optimization of the molecule was obtained by DFT modeling method using B3LYP/3-21g basis set and the same has been visualized with atom numbering in Fig. 5. The optimized molecule resembles a hat-shaped structure symmetric between two benzazepine units, unlike the horse-shoe shaped Ivabradine molecule. The benzene ring is distorted a bit as seen by the bond angles 118.9° and 119° at C1 and C6 positions respectively due to the presence of electron-releasing methoxy groups. Further, the methoxy substitution reduces the bond lengths between C1–C2 and C5–C6 to 1.39Å. The lactam chair is expectedly non-planar with bond angles of either 119° or 112° but with an increased bond angle of around 130° at N12. Further, there is a substantial reduction of bond length to 1.37 from 1.5Å between N12 and the beta carbon. There are considerable

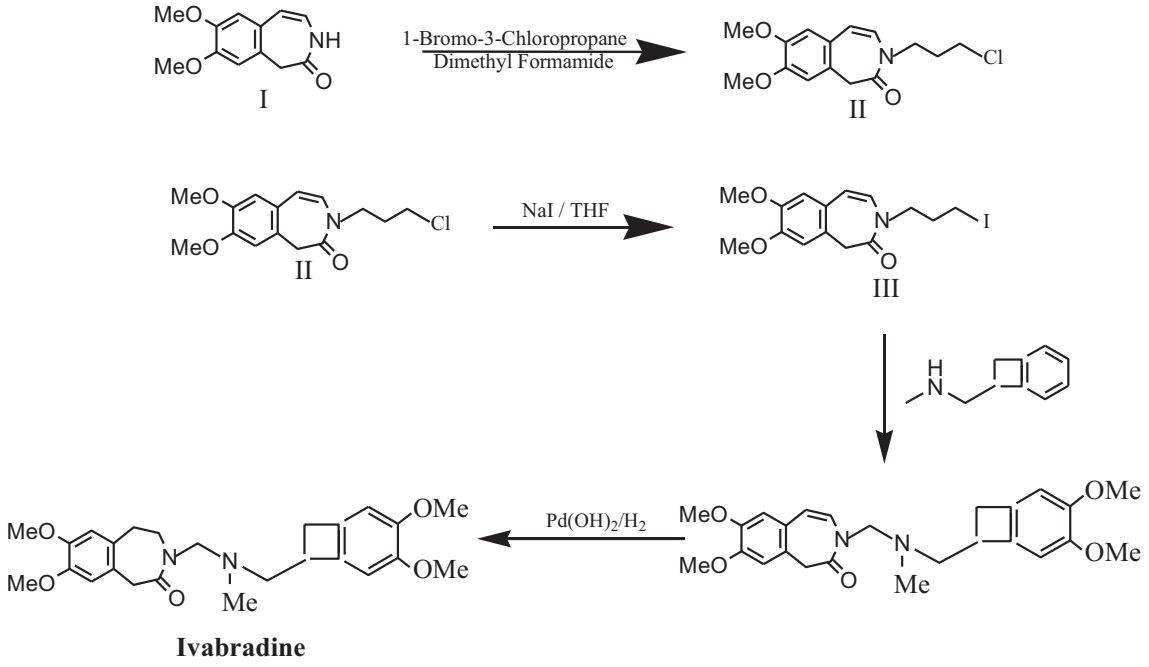

Fig. 2. Literature method for the synthesis of Ivabradine [19].

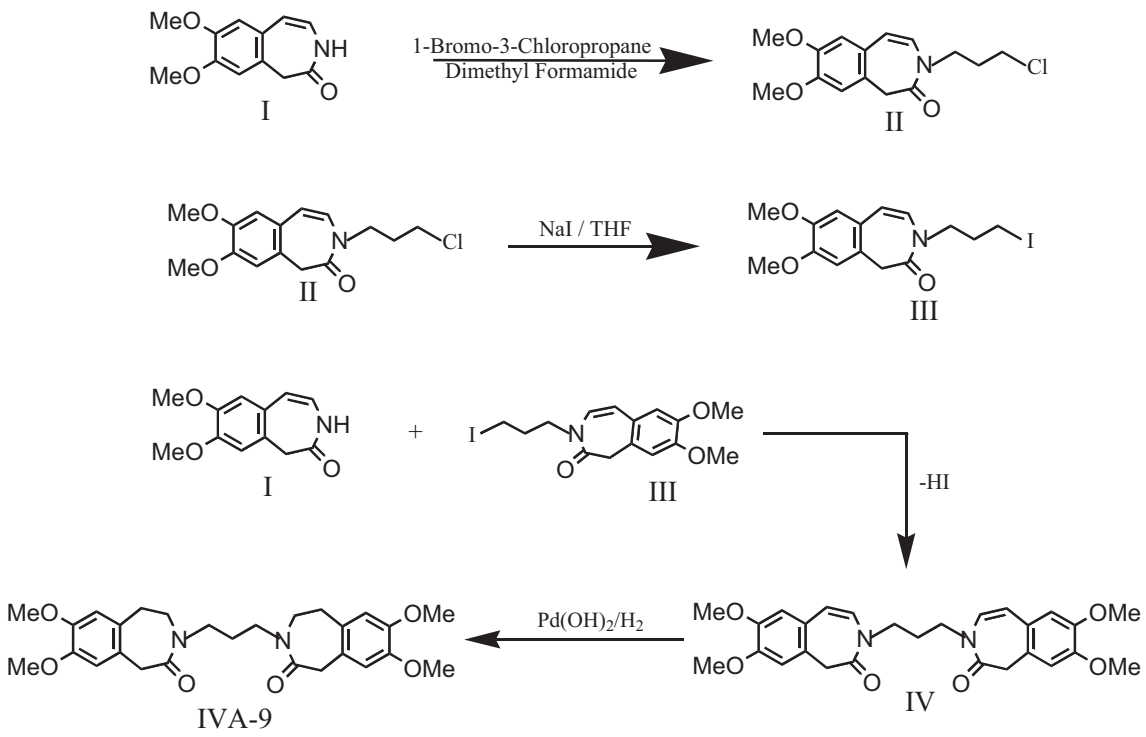

Fig. 3. Suggestive reaction route for the formation of IVA-9.

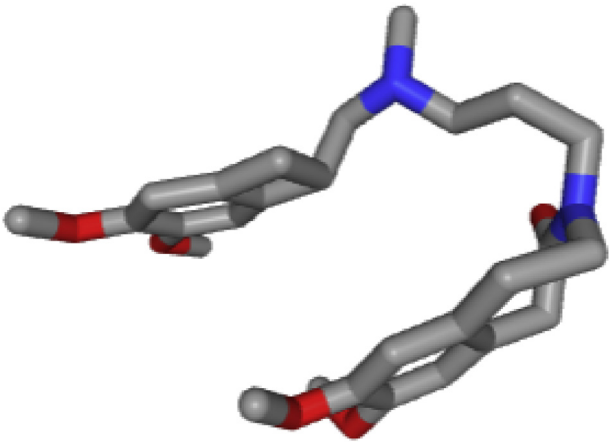

Fig. 4. Horse-shoe shaped form of Ivabradine (Image Credit: National Center for Biotechnology Information. PubChem Database [20]).

changes in bond angles at C10–N12–C11 (from 122° to 129.8°), at C10–N12–C13 (from 118.6° to 113.14°), at C11–N12–C13 (from 119.2° to 117°) and at N12–C13–C14 (from 112.2° to 115.4°) compared to Ivabradine molecule. These are presumably due to the replacement of cyclobutane segment by the repeat lactam unit here. The methoxy anisole groups on either side lie in more or less the same plane while the lactam units jut out at around 110° at halfway as shown by the dihedral angles. The apex of the hat made by the aliphatic linkage showed a bond angle of 116°. Out of the four methoxy groups, two (one each on either side) lie in the same plane as the benzene ring while other two (one each on either side) is out of the plane at a dihedral angle of 55° due to the possible torsional strains. The optimized structure visualizes that the lone pair on the lactam nitrogen delocalizes into the lactam ring. This has been corroborated by a short bond length of 1.37Å between N12 and C11. The list of significant dihedral angles is appended in below in Table 1.

The computed geometrical parameters such as bond lengths and bond angles were then compared with the experimentally obtained results. As no crystallographic data was available for IVA-9 in the literature, we have used the data pertaining to the lactam bearing segment of Ivabradine **[21]** for comparison. The results showed reasonable agreement between computed and experimental data (Table 2; Figs. 6 and 7).

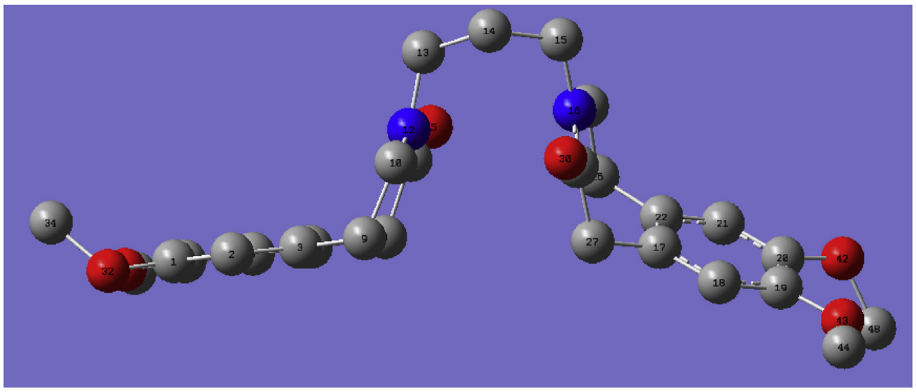

Fig. 5. Optimized geometry visualized at DFT/B3LYP/6-311g (H atoms being omitted for the sake of clarity).

Table 1
Consolidated list of Dihedral angles in IVA-9.

Sl. No	Dihedral	Angle (°)	Sl. No	Dihedral	Angle (°)
1	C6–C1–C2–C3	-0.49	40	C14–C15–N16–C29	-62.34
2	O32–C1–C2–C3	177.09	41	C15–N16–C28–C26	-176.58
3	C2–C1–C6–C5	-0.39	42	C29–N16–C28–C26	7.60
4	C2–C1–C6–O33	179.16	43	C15–N16–C29–C27	-178.42
5	O32–C1–C6–C5	-177.81	44	C15–N16–C29–O30	3.16
6	O32–C1–C6–O33	1.74	45	C28–N16–C29–C27	-2.70
7	C2–C1–O32–C34	127.61	46	C28–N16–C29–O30	178.87
8	C6–C1–O32–C34	-54.93	47	C22–C17–C18–C19	0.01
9	C1–C2–C3–C4	0.95	48	C27–C17–C18–C19	-179.79
10	C1–C2–C3–C9	179.15	49	C18–C17–C22–C21	0.96
11	C2–C3–C4–C5	-0.53	50	C18–C17–C22–C26	-176.96
12	C2–C3–C4–C8	177.83	51	C27–C17–C22–C21	-179.23
13	C9–C3–C4–C5	-178.83	52	C27–C17–C22–C26	2.85
14	C9–C3–C4–C8	-0.47	53	C18–C17–C27–C29	108.88
15	C2–C3–C9–C10	-108.03	54	C22–C17–C27–C29	-70.93
16	C4–C3–C9–C10	70.20	55	C17–C18–C19–C20	-0.90
17	C3–C4–C5–C6	-0.34	56	C17–C18–C19–O43	178.71
18	C8–C4–C5–C6	-178.65	57	C18–C19–C20–C21	0.80
19	C3–C4–C8–C11	-73.25	58	C18–C19–C20–O42	178.11
20	C5–C4–C8–C11	105.07	59	O43–C19–C20–C21	-178.84
21	C4–C5–C6–C1	0.80	60	O43–C19–C20–O42	-1.53
22	C4–C5–C6–O33	-178.71	61	C18–C19–O43–C44	-3.70
23	C1–C6–O33–C38	-177.67	62	C20–C19–O43–C44	175.92
24	C5–C6–O33–C38	1.85	63	C19–C20–C21–C22	0.19
25	C4–C8–C11–N12	54.54	64	C19–C20–C21–C24	179.60
26	C4–C8–C11–O25	-123.58	65	O42–C20–C21–C22	-177.28
27	C3–C9–C10–N12	-48.79	66	O42–C20–C21–C24	2.13
28	C9–C10–N12–C11	-14.74	67	C19–C20–O42–C48	55.53
29	C9–C10–N12–C13	166.80	68	C21–C20–O42–C48	-127.13
30	C8–C11–N12–C10	11.06	69	C20–C21–C22–C17	-1.07
31	C8–C11–N12–C13	-170.53	70	C20–C21–C22–C26	176.76
32	O25–C11–N12–C10	-170.89	71	C24–C21–C22–C17	179.54
33	O25–C11–N12–C13	7.52	72	C24–C21–C22–C26	-2.63
34	C10–N12–C13–C14	61.87	73	C17–C22–C26–C28	69.66
35	C11–N12–C13–C14	-116.80	74	C21–C22–C26–C28	-108.18
36	N12–C13–C14–C15	78.64	75	C22–C26–C28–N16	-61.90
37	C13–C14–C5–N16	-51.41	76	C17–C27–C29–N16	54.15
38	C13–C14–C5–N16	-51.41	77	C17–C27–C29–O30	-127.38
39	C14–C15–N16–C28	121.18			

Table 2
Geometrical parameters compared (Computed Vs Experimental [21]).

Parameter	Computed	Exptl (Ref)
Bond length (Å)		
C1–C2	1.39	1.37
C1–C6	1.41	1.40
C1–O32	1.39	1.38
C2–C3	1.40	1.41
C3–C4	1.40	1.39
C3–C9	1.51	1.52
C4–C5	1.40	1.41
C4–C8	1.51	1.52
C5–C6	1.39	1.38
C6–O33	1.39	1.36
C8–C11	1.54	1.52
C9–C10	1.55	1.51
C10–N12	1.49	1.46
C11–N12	1.37	1.35
C11–O25	1.26	1.23
N12–C13	1.49	1.50
C13–C14	1.54	1.53
C14–C15	1.55	1.51
C15–N16	1.49	1.50
N16–C28	1.50	1.46
N16–C29	1.36	1.35
C17–C18	1.40	1.41
C17–C22	1.40	1.39
C17–C27	1.51	1.52
C18–C19	1.39	1.37
C19–C20	1.41	1.40
C19–O43	1.39	1.38
C20–C21	1.39	1.38
C20–O42	1.39	1.36
C21–C22	1.40	1.41
C22–C26	1.51	1.52
C26–C28	1.54	1.51
C27–C29	1.54	1.52
C29–O30	1.26	1.23
O32–C34	1.48	1.35
O33–C38	1.46	1.41
O42–C48	1.48	1.35
O43–C44	1.46	1.41
Bond angle (°)		
C2–C1–C6	118.91	119.70
C2–C1–O32	117.45	116.4
C6–C1–O32	123.59	123.90
C1–C2–C3	121.76	121.90
C2–C3–C4	119.15	118.92
C2–C3–C9	123.09	125.50
C4–C3–C9	117.74	116.20
C3–C4–C5	119.67	118.30
C3–C4–C8	118.58	116.28
C4–C5–C8	121.73	124.80
C4–C5–C6	121.12	122.30
C1–C6–C5	119.38	119.10
C1–C6–O33	116.58	115.50
C5–C6–O33	124.04	125.40
C4–C8–C11	111.79	116.70
C3–C9–C10	113.02	116.70
C9–C10–N12	118.61	112.50
C8–C11–N12	119.04	117.40
C8–C11–O25	118.62	120.50
N12–C11–O25	122.31	122.40
C10–N12–C11	129.84	122.00
C10–N12–C13	113.14	118.60
C11–N12–C13	117.01	119.20
N12–C13–C14	115.42	112.20
C13–C14–C15	116.18	109.70
C14–C15–N16	116.13	118.60
C15–N16–C28	113.03	118.60
C15–N16–C29	116.07	119.20
C28–N16–C29	130.79	122.00
C18–C17–C22	119.68	116.20
C18–C17–C27	121.42	124.80
C22–C17–C27	118.91	116.28
C17–C18–C19	121.21	122.30
C18–C19–C20	119.31	119.70
C18–C19–O43	124.10	125.40
C20–C19–O43	116.59	116.4
C19–C20–C21	118.89	119.70
C19–C20–O42	123.46	123.90
C21–C20–O42	117.59	116.4
C20–C21–C22	121.90	121.90
C17–C22–C21	119.00	118.92
C17–C22–C26	118.46	116.20
C21–C22–C26	122.51	125.50
C22–C26–C28	112.32	116.70
C17–C27–C29	114.37	116.70
N16–C28–C26	117.68	112.50
N16–C29–C27	120.45	117.40
N16–C29–O30	120.92	122.40
C27–C29–O30	118.61	120.50
C1–O32–C34	116.82	117.60
C6–O33–C38	117.92	117.50
C20–O42–C48	116.61	117.60
C19–O43–C44	117.87	117.50

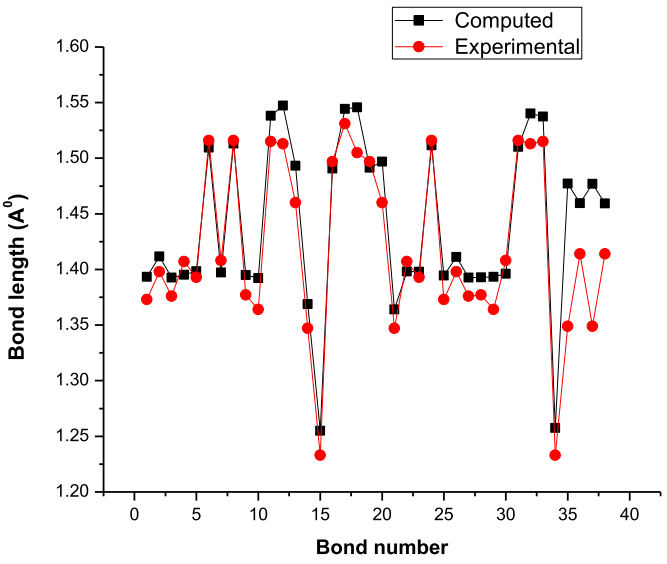

Fig. 6. Bond lengths compared (IVA-9).

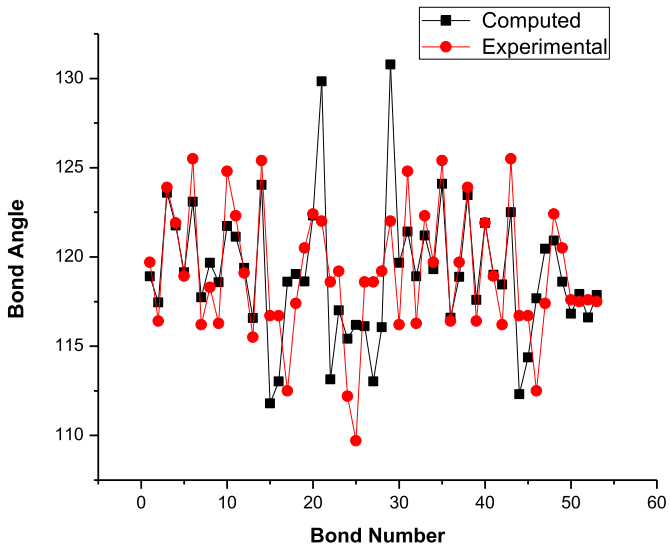

Fig. 7. Bond angles compared (IVA-9).

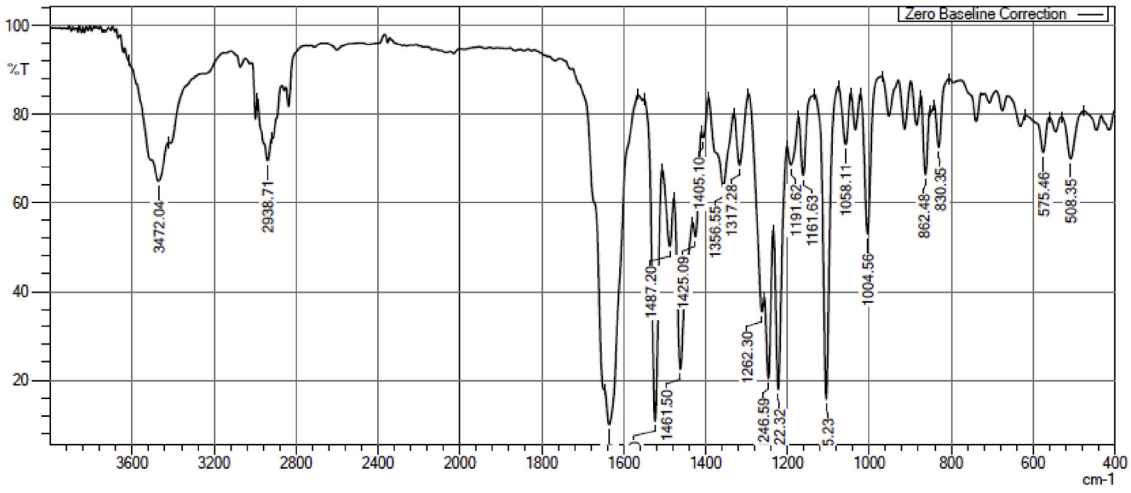

(a)

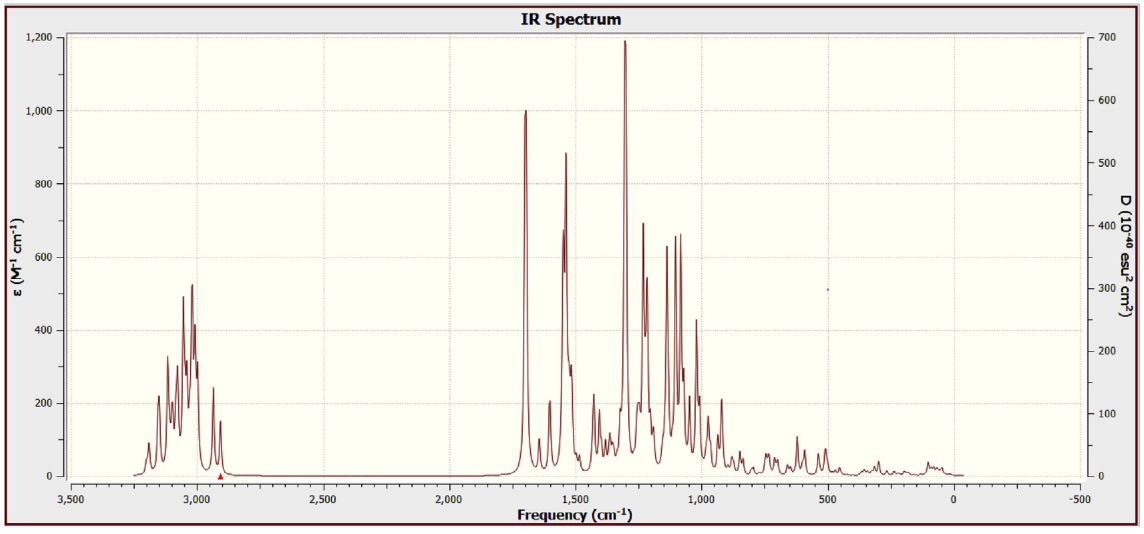

(b)

Fig. 8. (a): Experimental FTIR spectrum of IVA-9. (b): Computed IR Spectra of IVA-9 @ DFT-B3LYP/6-311g.

3.3. Vibrational studies

The solid phase FTIR spectrum was recorded using Shimadzu IRSpirit Fourier Transform Spectrophotometer and the fundamental modes of vibrations were analyzed and interpreted. KBr pellet method was used for sample preparation and the scanning was done between 4000-400 cm^{-1} with a resolution of 2 cm^{-1}. The vibrational frequencies were also computed using Gaussian09 with the optimized molecule geometry predicted by DFT at B3LYP/3-21g as the input. The optimized IVA-9 molecule has 69 atoms and 201 possible fundamental vibrations. The computed CH vibrational frequencies are scaled with a scaling factor of 0.966 for better agreement (See Fig. 8 (a) & (b); Table 3).

Aromatic CH stretching vibrations are observed between 3100-3000 cm^{-1} [22,23] and corresponding in-plane bending vibrations are seen in the range of 1400–1100 cm^{-1} **[24]** . Theoretical calculations show CH stretching vibrations at 3144.7, 3143.7, 3134.8 and 3134.2 cm^{-1} in-plane bending vibrations at 1319.2, 1315.3, 1297, 1289.6, 1289, 1286.6, 1281.4 and 1268.3 cm^{-1}. Though no peaks are observed for CH stretching vibrations in the experimental FTIR spectrum, a characteristic peak at 1317.2 cm^{-1} is seen corresponding to CH in-plane bending. The out of plane bending vibrations are recorded theoretically at 1147.7, 1138.8, 1123.4, 1102.1, 1100.1, 1098.6, 1096 and 1093.1 cm^{-1} while the equivalent experimental value is observed at 1105 cm^{-1}.

CO stretching shows up as strong bands between 1850-1600 cm^{-1}

Table 3
Vibrational frequencies and interpretations.

Sl No	Wave number	Scaled wave No	Int.	Assignment	Experimental
1	3201.511	3092.7	9.7	Ar CH str Sym	
2	3197.202	3088.5	4.1	Ar CH str Sym	
3	3190.851	3082.4	18.9	Ar CH str Sym	
4	3188.837	3080.4	12.0	Ar CH str Sym	
5	3155.395	3048.1	21.4	Asymm CH_3 str	
6	3153.901	3046.7	23.5	Asymm CH_3 str	
7	3149.812	3042.7	29.1	Asymm CH_3 str	
8	3149.051	3042.0	29.6	Asymm CH_3 str	
9	3116.002	3010.1	37.2	Asymm CH_3 str	
10	3115.972	3010.0	65.1	Asymm CH_3 str	
11	3111.785	3006.0	18.2	Asymm CH_2 str (heterocyclic)	
12	3107.048	3001.4	14.3	Asymm CH_2 str (heterocyclic)	
13	3099.331	2994.0	42.1	Asymm CH_2 str (heterocyclic)	
14	3095.226	2990.0	28.4	Asymm CH_2 str	
15	3083.884	2979.0	43.2	Asymm CH_2 str	
16	3078.533	2973.9	48.8	CH_3 str (terminal)	
17	3075.533	2971.0	52.6	CH_3 str (terminal)	
18	3054.863	2951.0	73.4	Asymm CH_2 str (heterocyclic)	
19	3054.102	2950.3	81.3	Asymm CH_2 str (heterocyclic)	
20	3048.506	2944.9	47.1	CH_2 str (ali. link)	
21	3042.372	2938.9	12.4	CH_2 str (ali. link)	
22	3040.811	2937.4	51.3	Sym CH_2 str (heterocyclic)	2910
23	3038.876	2935.6	11.0	Sym CH_2 str (heterocyclic)	
24	3038.367	2935.1	15.4	Sym CH_2 str (heterocyclic)	
25	3029.112	2926.1	33.1	Sym CH_2 str (heterocyclic)	
26	3021.047	2918.3	91.6	CH_3 str (terminal)	
27	3018.441	2915.8	102.8	CH_3 str (terminal)	
28	3017.135	2914.6	3.7	CH_2 str (ali. link)	
29	3008.44	2906.2	62.6	CH_3 str (terminal)	
30	3006.933	2904.7	62.6	CH_3 str (terminal)	
31	2998.262	2896.3	46.0	Sym CH_2 str (heterocyclic)	
32	2996.442	2894.6	53.1	Sym CH_2 str (heterocyclic)	
33	2935.188	2835.4	92.3	CH_2 str (ali. link)	
34	2906.904	2808.1	57.0	CH_2 str (ali. link)	
35	1699.808	1642.0	486.3	C=O str	
36	1694.602	1637.0	477.0	C=O str	
37	1644.074	1588.2	33.8	C–C str (ring)	
38	1642.185	1586.4	33.3	C–C str (ring)	
39	1603.122	1548.6	73.6	C–C str (ring)	
40	1600.325	1545.9	90.6	C–C str (ring)	
41	1556.677	1503.8	10.5	CH_2 str (ali. link)	
42	1549.853	1497.2	190.4	Scis CH_3	
43	1548.451	1495.8	155.5	Scis CH_3	
44	1545.943	1493.4	81.4	Scis CH_3	
45	1545.162	1492.6	67.1	Scis CH_3	
46	1543.005	1490.5	1.0	Scis CH_2 (ali)	
47	1537.757	1485.5	265.1	Scis CH_3	1650
48	1536.855	1484.6	319.0	Scis CH_3	
49	1531.053	1479.0	17.0	Scis CH_2 (ali)	
50	1526.479	1474.6	28.5	Scis CH_3	
51	1526.412	1474.5	25.0	Bending CH_3	
52	1524.926	1473.1	46.9	Scis CH_2 (heterocy)	
53	1522.555	1470.8	36.9	Scis CH_2 (heterocy)	
54	1518.395	1466.8	13.6	Scis CH_2 (heterocy)	
55	1517.876	1466.3	34.9	Scis CH_2 (heterocy)	
56	1516.327	1464.8	41.7	Scis CH_2 (heterocy)	1635
57	1516.06	1464.5	39.4	Scis CH_3 (ter)	
58	1513.305	1461.9	55.6	Scis CH_2 (heterocy)	
59	1512.914	1461.5	25.5	Scis CH_2 (heterocy)	
60	1497.037	1446.1	13.2	OCH_3 bending	
61	1495.898	1445.0	9.8	OCH_3 bending	
62	1484.674	1434.2	13.1	OCH_3 bending	
63	1483.32	1432.9	19.7	OCH_3 bending	
64	1433.963	1385.2	17.1	CH_2 wagging	
65	1429.671	1381.1	56.6	CH_2 wagging	
66	1426.64	1378.1	96.0	CH_2 wagging	
67	1424.612	1376.2	44.0	CH_2 wagging	
68	1405.085	1357.3	128.7	CH_2 wagging	
69	1396.42	1348.9	45.7	CH_2 wagging (heterocyclic)	1523
70	1383.794	1336.7	12.5	CH_2 wagging (heterocyclic)	
71	1379.82	1332.9	55.9	CH_2 wagging (heterocyclic)	1487
72	1366.752	1320.3	29.9	CH_2 wagging (heterocyclic)	
73	1362.713	1316.4	61.4	CH_2 twist	1460
74	1354.392	1308.3	30.0	CH_2 twist	
75	1351.528	1305.6	14.0	CH_2 wagging (heterocyclic)	
76	1348.045	1302.2	29.2	CH_2 wagging (heterocyclic)	
77	1336.181	1290.8	9.3	CH_2 wagging (heterocyclic)	
78	1334.796	1289.4	10.3	CH_2 wagging (heterocyclic)	
79	1323.181	1278.2	94.7	CH_2 out of plane bend	1422
80	1316.388	1271.6	23.1	CH inplane bend	1405
81	1307.107	1262.7	75.1	CH inplane bend	
82	1305.663	1261.3	108.4	CH inplane bend	
83	1304.04	1259.7	591.0	CH inplane bend	
84	1299.376	1255.2	698.1	CH_2 out of plane bend	
85	1268.98	1225.8	16.3	CH_2 out of plane bend	
86	1256.817	1214.1	79.7	CH_3 out of plane bend, CH_2 twist	1355
87	1252.067	1209.5	78.0	CH_2 twist	
88	1247.457	1205.0	50.9	CH in plane bend	1317
89	1245.062	1202.7	47.6	CH in plane bend	
90	1231.01	1189.2	567.8	CH in plane bend	
91	1224.329	1182.7	99.8	CH in plane bend	
92	1218.057	1176.6	140.1	CH in plane bend	
93	1215.326	1174.0	346.7	CH in plane bend	

(*continued on next page*)

Table 3 (*continued*)

Sl No	Wave number	Scaled wave No	Int.	Assignment	Experimental
94	1204.083	1163.1	6.1	CH in plane bend	
95	1202.937	1162.0	39.6	CH in plane bend	
96	1202.361	1161.5	56.1	CH in plane bend	1261
97	1191.733	1151.2	65.9	CH_3 twist	
98	1188.306	1147.9	39.6	CH_3 twist	
99	1159.176	1119.8	1.8	CH_3 twist	
100	1159.099	1119.7	2.7	CH_3 twist	1246.5
101	1154.938	1115.7	25.4	CH in plane bend	
102	1153.454	1114.2	23.5	CH in plane bend	
103	1146.305	1107.3	48.5	CN stretching	1222.3
104	1137.087	1098.4	579.3	CN stretching	1191
105	1131.124	1092.7	95.0	CH_2 twist	
106	1116.073	1078.1	45.5	CN stretching	1161
107	1102.798	1065.3	418.9	CH_2 twist	
108	1102.324	1064.8	224.9	CN stretching	
109	1082.459	1045.7	646.2	CH out of plane bend	
110	1070.67	1034.3	225.2	CH out of plane bend	
111	1057.96	1022.0	13.8	CH out of plane bend	
112	1047.602	1012.0	206.3	CH out of plane bend	1105
113	1020.344	985.7	389.9	CH out of plane bend	
114	1017.745	983.1	89.2	CH out of plane bend	
115	1007.925	973.7	188.4	CH out of plane bend	
116	993.5127	959.7	10.8	CH out of plane bend	
117	986.0881	952.6	16.1	OCH_3 Str	1058
118	981.015	947.7	51.9	OCH_3 Str	
119	973.1914	940.1	158.4	OCH_3 Str	
120	964.3691	931.6	73.8	OCH_3 Str	
121	935.4415	903.6	115.5	OCH_3 Str	
122	921.4069	890.1	105.4	OCH_3 Str	
123	919.4756	888.2	111.3	OCH_3 Str	
124	918.5779	887.3	55.4	CH out of plane bend	
125	912.3955	881.4	10.4	OCH_3 Str	1003.8
126	895.2635	864.8	25.0	CH_2 out of plane bend (heterocyclic)	
127	884.7871	854.7	6.7	CH_2 out of plane bend (heterocyclic)	
128	879.6443	849.7	52.1	CH_2 out of plane bend (heterocyclic)	
129	872.7831	843.1	34.0	CH_2 out of plane bend (heterocyclic)	
130	847.7777	819.0	83.0	CH out of plane bend	
131	835.5793	807.2	56.5	CH out of plane bend	
132	802.8441	775.5	20.1	CH_2 out of plane bend	
133	794.9082	767.9	27.7	CH_2 out of plane bend (heterocyclic)	863
134	771.6454	745.4	11.0	CH_2 out of plane bend (heterocyclic)	
135	748.4924	723.0	30.1	CH_2 out of plane bend (heterocyclic)	
136	744.2697	719.0	63.8	CH_2 out of plane bend (heterocyclic)	830.5
137	736.1454	711.1	38.0	CH out of plane bend	
138	732.2824	707.4	63.0	CH out of plane bend	
139	720.3195	695.8	3.0	CH bend in plane	
140	710.029	685.9	68.7	CH bend in plane	
141	703.002	679.1	19.4	CH bend in plane	
142	697.8704	674.1	55.2	CH_2 out of plane bend (heterocyclic)	
143	659.869	637.4	48.7	CH_2 out of plane bend (heterocyclic)	
144	647.6128	625.6	37.0	CH_2 out of plane bend (heterocyclic)	
145	620.7038	599.6	196.5	CH_2 out of plane bend (heterocyclic)	
146	600.414	580.0	30.6	CH_2 out of plane bend (heterocyclic)	
147	599.2496	578.9	22.4	C–C–C in plane bend	
148	590.8451	570.8	126.6	C–C–C in plane bend	
149	536.8585	518.6	124.3	C–C–C in plane bend	
150	528.9297	510.9	16.1	C–C–C in plane bend	
151	510.1825	492.8	120.4	C–C–C in plane bend	
152	506.4279	489.2	70.3	C–C–C in plane bend	
153	500.1282	483.1	51.7	C–C–C in plane bend	575
154	492.2831	475.5	6.9	C–C–C in plane bend	
155	481.0087	464.7	16.5	C–C–C in plane bend	
156	469.9999	454.0	34.4	C–C–C in plane bend	
157	453.2236	437.8	54.3	C–C–C in plane bend	
158	444.1604	429.1	10.5	C–C–C in plane bend	
159	427.2545	412.7	5.5	C–C–C in plane bend	
160	416.7383	402.6	3.0	C–C–C in plane bend	
161	400.3562	386.7	6.8	C–C–C in plane bend	
162	373.8254	361.1	5.6	C–C–C in plane bend	
163	366.7925	354.3	26.7	C–C–C in plane bend	
164	357.1741	345.0	36.5	C–C–C in plane bend	
165	352.9152	340.9	23.7	C–C–C in plane bend	
166	342.067	330.4	39.9	C–C–C in plane bend	
167	326.9119	315.8	38.2	C–C–C in plane bend	
168	314.4024	303.7	88.3	C–C–C in plane bend	
169	299.4024	289.2	23.4	C–C–C in plane bend	
170	297.1623	287.1	132.5	C–C–C in plane bend	
171	271.9593	262.7	6.1	C–C–C out of plane bend	
172	265.011	256.0	58.5	C–C–C out of plane bend	
173	253.7061	245.1	3.8	C–C–C out of plane bend	
174	237.5253	229.4	54.4	C–C–C out of plane bend	
175	232.2319	224.3	14.9	C–C–C out of plane bend	
176	219.7438	212.3	34.2	C–C–C out of plane bend	
177	209.9424	202.8	10.2	C–C–C out of plane bend	
178	197.4085	190.7	50.4	C–C–C out of plane bend	
179	196.6722	190.0	12.6	C–C–C out of plane bend	
180	188.5958	182.2	45.7	C–C–C out of plane bend	
181	178.1327	172.1	46.9	C–C–C out of plane bend	
182	160.2606	154.8	10.8	C–CH_3 in plane bend	
183	153.0272	147.8	5.9	C–CH_3 in plane bend	
184	149.0355	144.0	5.4	C–CH_3 in plane bend	
185	130.7146	126.3	42.8	C–CH_3 in plane bend	
186	109.4655	105.7	23.2	C–CH_3 in plane bend	
187	102.45	99.0	305.7	C–CH_3 in plane bend	
188	100.2459	96.8	93.6	C–CH_3 in plane bend	
189	91.6622	88.5	62.4	C–CH_3 in plane bend	
190	89.2848	86.2	181.9	C–CH_3 in plane bend	
191	79.5637	76.9	285.8	C–CH_3 in plane bend	
192	68.2426	65.9	274.5	C–CH3 in plane bend	
193	61.6222	59.5	78.8	C–CH3 in plane bend	
194	60.5378	58.5	115.2	C–CH3 in plane bend	
195	53.7358	51.9	155.9	C–CH3 in plane bend	
196	46.6306	45.0	482.4	twisting	
197	35.7936	34.6	102.7	twisting	
198	18.7934	18.2	201.7	twisting	
199	14.5906	14.1	194.4	twisting	
200	10.681	10.3	148.5	twisting	
201	7.6	7.3	86.0	twisting	

and the computed peaks at 1807, 1796, 1778, 1773, 1767, 1743, 1691 and 1658 cm^{-1} are assigned to this. The broad twin peak at 1635 cm^{-1} in the FTIR is ascribed to CO stretching. The corresponding in-plane bending is seen as weak bands at 955 and 925 cm^{-1} whereas the out of plane bending is seen at 786 and 763 cm^{-1} as strong bands. The characteristic peaks for methoxy groups are seen at around 1250 and 1050 cm^{-1}. The corresponding peaks are computed at 1289, 1286, 1281, 1268, 1257.8, 1257.7, 1250.5, 1250.4 and 1059, 1057, 1052, 1044, 1039, 1034, 1023, 1001, 999 cm^{-1} respectively. FTIR peaks at 1355, 1313 & 1058, 1003 cm^{-1} are indicative of this. The strong peak at 2849 cm^{-1} in the experimental spectrum is typical of methylene asymmetric stretching in the heterocyclic ring. Same bands are visualized at 2934 and 2841 cm^{-1} in theoretical calculation. The characteristic CN stretching

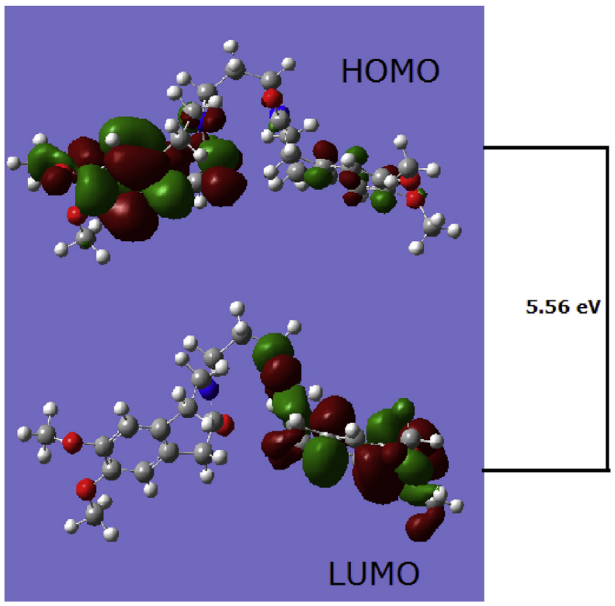

Fig. 9. HOMO-LUMO energy gap.

vibrations are visible at 1237, 1194 cm^{-1} and 1227, 1191 cm^{-1} in theoretical and experimental analysis respectively.

3.4. HOMO-LUMO energy gap

The energies of frontier orbitals are useful in assessing the chemical reactivity and thermodynamic stability of a system (See Fig. 9). In general, the energies of the highest occupied molecular orbital (HOMO) and the lowest unoccupied molecular orbital (LUMO) indicate the electron-releasing and electron-gaining capacities respectively. The HOMO and LUMO energies of 7,8-dimethoxy-1,3-dihydrobenzo(d)azepin-2-one (I) & 7,8-Dimethoxy-3-(3-iodopropyl)-l, 3-dihydro-2H-3-benzazepin-2-one (III), the addition product (IV) and IVA-9 are computed and presented in Table 4.

A relatively larger HOMO-LUMO gap of 5.56 eV in IVA-9 is justifiable due to a relatively small aromatic system compared to the reagent compounds and intermediates. Due to this, IVA-9 shows higher kinetic and thermodynamic stability and less chemical reactivity. Further, the lack of conjugation renders the molecule colorless with fewer chances of electronic excitation in the visible range.

The energy gap of 5.56 eV in IVA-9 falls at around 225 nm in the ultraviolet region and the molecule is expected to show strong absorption at this wavelength. This has been cross-checked by performing UV-Visible scan via experimental (using Shimadzu UV-Vis spectrophotometer) and computational Time-Dependent DFT (TDDFT) methods and the results are given below (Fig. 10).

A relatively smaller electronic energy implies good stability of the impurity molecule compared to other reacting intermediates and the possibility of the molecule being carried over along with the active ingredient during commercial synthesis.

Table 4
HOMO-LUMO Energy gap.

Compound	HOMO (eV)	LUMO (eV)	ΔE (eV)	Dipole moment (D)	Electronic energy (eV)
Compound I	-5.83	-1.06	4.77	3.12	-27,170.70
Compound III	-5.89	-1.34	4.54	3.37	-2,8,844.43
Addition product IV	-4.91	-2.86	2.05	2.89	-43,499.50
IVA-9	-5.40	0.16	5.56	1.39	-43,572.97

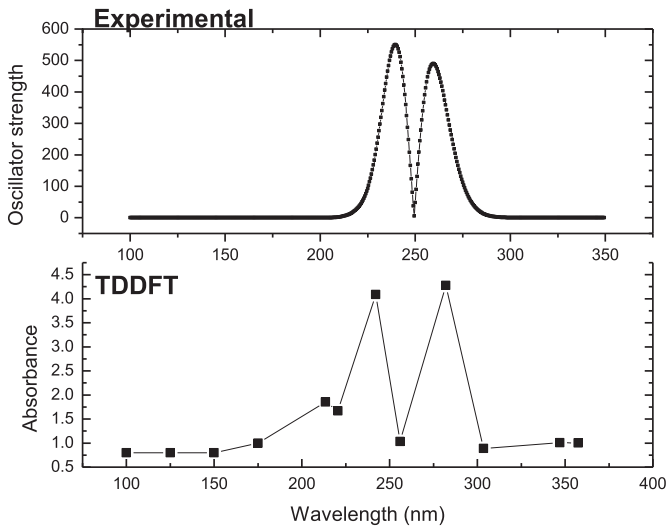

Fig. 10. UV-Visible spectrum of IVA-9.

3.5. ADME studies

Safety and efficacy are vital aspects of the drug discovery process. It is important to know how the human body process and reacts to a drug system. A successful drug molecule must reach the target site in the adequate amount and remain there in its bioactive form till its intended biologic actions are performed. The evaluation of parameters such as absorption, distribution, metabolism, and excretion (ADME) are very important in this regard for a potential drug molecule. Drug development pipeline often produces a myriad of impurity and intermediate molecules with a potential drug-like character and toxicity effects. The onus is the investigator to spot the best molecule that could go on to become a potential medicine. SwissADME is a useful tool for this primary level of screening and helps in reducing pharmacokinetics-related failure during clinical trials at a later stage [25]. The output file contains a 2D chemical structure of the compound and bioavailability radar which gives a quick inference about the drug-likeness in a nutshell (Fig. 11). Six parameters namely flexibility, lipophilicity, size, polarity, solubility and saturation and their critical limits are depicted in the bioavailability radar (See Table 5). SwissADME also provides insights into other pharmacokinetic properties such as human gastrointestinal absorption (HIA), blood-brain-barrier (BBB) permeability, total polar surface area (TPSA) and inhibitor action to important cytochromes, etc.

By and large, IVA-9 shows similar physiochemical properties compared to Ivabradine. The cytochrome inhibitory actions are similar in most cases. It has a slightly higher total polar surface area (TPSA) due to the presence of extra polar carbonyl oxygen. This, in turn, results in a lower blood-brain-barrier (BBB) permeability. Overall, both molecules show comparable drug-likeness and medicinal chemistry friendliness indices.

4. Conclusions

The structural, spectral and physiochemical properties of the title molecule were studied. The lattice parameters and IR intensities computed showed reasonable concordance with the experimental results pertaining to the lactam bearing segment of Ivabradine molecule. The prospects of chance formation of IVA-9 impurity during the commercial manufacture of the parent drug were also discussed. A relatively larger HOMO-LUMO gap of 5.56 eV shows higher kinetic and thermodynamic stability and less chemical reactivity. The physiochemical properties of IVA-9 such as lipophilicity, water-solubility, polarity, and saturation are comparable to that of the drug molecule, Ivabradine. However, the bioavailability radar shows IVA-9 relatively more flexible than the parent

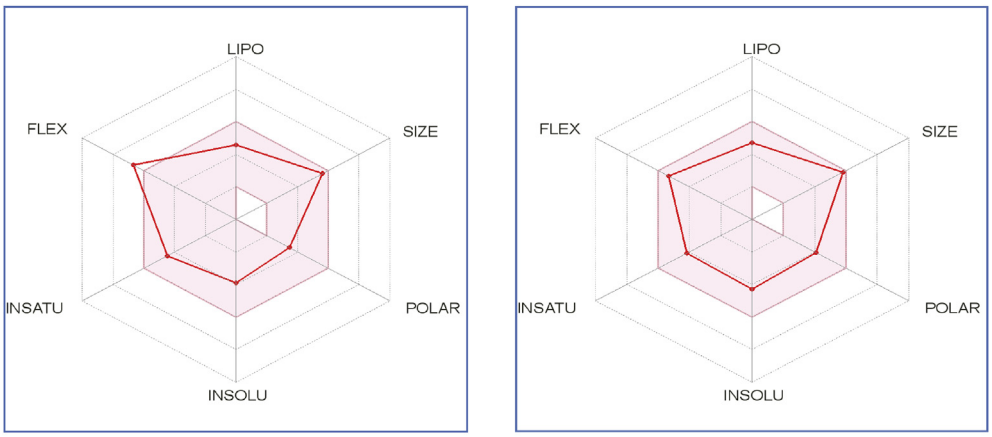

(a) (b)

Fig. 11. (a) Bio-availability radar-Ivabradine. (b): Bio-availability radar-IVA-9.

Table 5
Physiochemical parameters of Ivabradine and IVA-9.

Parameters	Ivabradine	IVA-9
No. of H bond acceptors	6	6
No. of H bond donors	0	0
Topological Polar Surface area, TPSA ($[Å]^2$)	60.5	77.5
Lipophilicity, log P	3.4	2.99
Water Solubility, log S	-3.9	-4.2
GI absorption	High	High
BBB permeant	Yes	No
P-gp substrate	Yes	Yes
CYP1A2 inhibitor	No	No
CYP2C19 inhibitor	No	Yes
CYP2C9 inhibitor	No	Yes
CYP2D6 inhibitor	Yes	Yes
CYP3A4 inhibitor	Yes	Yes
Skin permeation, log K_P (Cm/S)	-7.37	-7.31
Drug-likeness	Yes	Yes

drug due to its symmetric structure. This could be a factor considering the fact that Ivabradine physically binds to the HCN channels to block the passage of ions. It would be useful to explore the possibility of using the impurity molecule for selective blocking in HCN channels due to the structural appropriateness. As a future scope, the article envisages the toxicity studies of the impurity when present along with the parent drug in pharmacological formulations.

Declarations

Author contribution statement

S Anil Kumar: Performed the experiments; Analyzed and interpreted the data; Contributed reagents, materials, analysis tools or data; Wrote the paper.

B.L Bhaskar: Conceived and designed the experiments; Analyzed and interpreted the data.

Funding statement

This research did not receive any specific grant from funding agencies in the public, commercial, or not-for-profit sectors.

Competing interest statement

The authors declare no conflict of interest.

Additional information

No additional information is available for this paper.

References

[1] A. Satinder, Impurities Evaluation of Pharmaceuticals, Marcel Dekker, New York, 1998.
[2] A. Bucchi, A. Tognati, R. Milanesi, M. Baruscotti, D. DiFrancesco, Properties of Ivabradine-induced block of HCN1 and HCN4 pacemaker channels, J. Physiol. 572 (2006) 335–346.
[3] J.S. Koruth, A. Lala, S. Pinney, V.Y. Reddy, S.R. Dukkipati, The clinical use of Ivabradine, J. Am. Coll. Cardiol. 70 (2017) 1777–1784.
[4] J. Nowakowska, P. Pikul, M. Marszall, K. Ciura, Application and validation of simple isocratic HPLC-UV-DAD method with dual wavelength detection for Ivabradine determination and its application in the study of stress degradation, J. Chem. (2017), 2069571, 1-7.
[5] D. Duval, P. Hennig, J.P. Bouchet, J. Vian, J.L. Peglion, J.P. Volland, N. Platzer, J. Guilhem, Stereochemical study of a bradicardisant benzazepine type drug – X-ray structure of the chloride salt and high field NMR study of the stereochemistry in solution, Magn. Reson. Chem. 35 (1997) 175–183.
[6] N. Masciocchi, A. Aulisio, G. Bertolini, M. Sada, F. Garis, L. Malpezzi, Disclosing the extensive crystal chemistry of Ivabradine hydrochloride in its pure and solvated phases, Powder Diffr. 28 (2013) 200–206.
[7] V. ládková, O. Dammer, G. Sedmak, E. Skořepová, B. Kratochvíl, Ivabradine hydrochloride (S)-mandelic acid co-crystal: in situ preparation during formulation, Crystals 7 (2017) 13.
[8] P. Klippert, J.P. Jeanniot, S. Polvé, C. Lefèvre, H. Merdjan, Determination of Ivabradine and its N-demethylated metabolite in human plasma and urine, and in rat and dog plasma by a validated high-performance liquid chromatographic method with fluorescence detection, J. Chromatogr. B Biomed. Sci. Appl. 719 (1998) 125–133.
[9] S. Maheshwari, A.P. Khandhar, A. Jain, Quantitative determination and validation of Ivabradine HCL by stability indicating RP-HPLC method and spectrophotometric method in solid dosage form, Eurasian J. Anal. Chem. 5 (2010) 53–62.
[10] P. Pikul, J. Nowakowska, K. Ciura, Chromatographic analysis of Ivabradine on polar, nonpolar and chemically modified adsorbents by HPTLC, J. Food Drug Anal. 21 (2013) 165–168.
[11] P. Pikul, J. Nowakowska, K. Ciura, Effect of non-aqueous and buffered mobile phase composition on the retention of Ivabradine, J. Liq. Chromatogr. Relat. Technol. 37 (2014) 1837–1846.
[12] X. Jin, C.T. Lu, Y.L. Feng, L.K. Ding, Y. Guan, W. Sun, L. Zhou, A.D. Wen, Determination of Ivabradine in human plasma by LC-MS/MS and study of pharmacokinetics, Prog. Mod. Biomed. 14 (2011) 2605–2608.
[13] C. Lu, Y. Jia, J. Yang, X. Jin, Y. Song, W. Liu, Y. Ding, X. Sun, A. Wen, Simultaneous determination of Ivabradine and N-desmethylIvabradine in human plasma and urine using a LC-MS/MS method: application to a pharmacokinetic study, Acta Pharm. Sin. B 2 (2012) 205–212.
[14] J. Jiang, L. Tian, Y. Huang, Y. Li, Development and validation of a sensitive LCMS/MS ESI method for the determination of Ivabradine in human plasma: application to a pharmacokinetic study, Biomed. Chromatogr. 27 (2013) 1603–1608.
[15] N.M. Mostafa, Y.M. Fayez, J.F. Farid, A.E.B. El-Alim, Stability indicating spectrophotometric methods for determination of Ivabradine hydrochloride in the presence of its degradation product, Anal. Chem. Lett. 7 (2018) 280–294.
[16] S.A. Kumar, B.L. Bhaskar, Spectroscopic and volumetric techniques for the estimation of Ivabradine impurity 3,3'-(propane-1,3-diyl)bis(7,8-dimethoxy-1,3,4,5-tetrahydro-2H-benzo[d]azepin-2-one), Int. J. Appl. Sci. 11 (3) (2019) 216–218.

[17] M.J. Frisch, G.W. Trucks, H.B. Schlegel, G.E. Scuseria, M.A. Robb, et al., Gaussian, Inc., Wallingford, CT, 2009.
[18] A. Daina, O. Michielin, V. Zoete, SwissADME: a free web tool to evaluate pharmacokinetics, drug-likeness and medicinal chemistry friendliness of small molecules, Nature Sci. Rep. 7 (42717) (2017) 1–13.
[19] K.K. Kiran, R. Srinivas, K.B. Sravan, P.V. Srinivas, Ivabradine Hydrochloride and the Process for Preparation Thereof, Patent – W02014/020534A1 WIPO (PCT), 2014.
[20] National Center for Biotechnology Information. PubChem Database, Ivabradine, CID=132999, https://pubchem.ncbi.nlm.nih.gov/compound/Ivabradine.
[21] Stable Hydrochloric Acid Ivabradine II crystal Form and Preparation Method, Patent – CN103183639B, 2011.
[22] R. Zwarich, J. Smolarck, L. Goodman, Assignment of out of plane vibrational modes in benzaldehyde, J. Mol. Spectrosc. 38 (1971) 336–357.
[23] N.P.G. Roeges, A Guide to Complete Interpretation of Infrared Spectrum of Organic Structures, Wiley, New York, 1994.
[24] N. Sundaraganesan, H. Umamaheswari, B. Dominic Joshua, C. Meganathan, M. Ramalingam, Molecular structure and vibrational spectra of indole and 5-aminoindole by density functional theory and ab initio Hartree–Fock calculations, J. Mol. Struct. 850 (2008) 84–93.
[25] M. Hay, D.W. Thomas, J. L Craighead, C. Economides, J. Rosenthal, Clinical development success rates for investigational drugs, Nat. Biotechnol. 32 (2014) 40–51.